EXES: A progress report on the development of a high-resolution, mid-infrared grating spectrograph for SOFIA.

M. J. Richter,[a] J. H. Lacy,[a] D. T. Jaffe,[a], T. K. Greathouse,[a] and M. K. Hemenway[a]

[a]University of Texas, Astronomy Department, Austin, TX 78712

ABSTRACT

We are developing a high spectral resolution grating spectrograph as a PI instrument for the Stratospheric Observatory for Infrared Astronomy (SOFIA). The Echelon-Cross-Echelle Spectrograph (EXES) will operate at 5.5-28.5 μm in three spectroscopic modes: R $\sim 10^5$, 2 $\times 10^4$, and 4000. We use an echelon, a coarsely ruled, steeply blazed diffraction grating to achieve high resolution. Cross-dispersion is done with an echelle used at relatively low order. The detector is a 256 $\times$ 256 pixel Si:As IBC array. A very similar instrument, the Texas Echelon-Cross-Echelle Spectrograph (TEXES), has had a successful telescope run at the McDonald Observatory. We give here a progress report on the design of EXES and the status of TEXES.

Keywords: Infrared, Spectrograph, SOFIA

1. INTRODUCTION

Molecules provide the best tracers of the changes in density, temperature, bulk velocity, and chemical state as diffuse clouds become stars with disks and planets. Our current picture of star formation has benefited greatly from molecular line observations at millimeter and sub-mm wavelengths. Molecular line observations in the infrared, where many important molecules have transitions, have been less useful because of limits imposed by the spectral resolution and sensitivity of existing spectrographs, and the opacity of the Earth's atmosphere. We are building a mid-infrared spectrograph that will, when used on the Stratospheric Observatory for Infrared Astronomy (SOFIA), push back those limits.

As discussed in a previous paper,[1] the echelon-cross-echelle spectrograph (EXES), is a versatile, PI-class instrument designed to take advantage of SOFIA's unique capabilities for observations of infrared molecular lines. EXES will operate at wavelengths from 5.5 μm to 28.5 μm, a spectral region with many molecular rotation-vibration transitions. In cross-dispersed mode, it will have a resolving power of R $\geq 10^5$ for $\lambda \leq 10$ μm and R $= 10^6/\lambda$ for $\lambda > 10$ μm to maximize sensitivity to the narrow lines expected from molecular clouds, and instantaneous wavelength coverage of 0.3% varying with wavelength. At altitudes reached by SOFIA, EXES will be able to observe H_2 and H_2O transitions that are totally blocked or heavily attenuated from the ground. EXES will also have medium (R$\sim 2 \times 10^4$) and low (R$\sim$4000) spectral resolution modes in a long-slit format. There will also be a camera mode suitable for target location. The detector is a 256^2 Si:As IBC array designed for low background operation.

EXES builds upon engineering and technical development done for its prototype, the Texas echelon-cross-echelle spectrograph (TEXES), a ground-based high resolution mid-infrared spectrograph. While the optical, mechanical, and thermal designs of the two instruments have slight differences, the detector, electronics, and software will be shared between the two. TEXES serves as a testbed for new technology and allows us to optimize and debug key system components well in advance of EXES's first SOFIA flights. TEXES recently had a successful observing run at the McDonald Observatory 2.7 meter Harlan J. Smith Telescope.

This paper describes the current state of the EXES design and the recent knowledge gained with TEXES. Where appropriate, we merely summarize the information given in earlier papers: notably a description of the echelon[2] and the science goals and sensitivity estimates for EXES.[1]

E-mail: richter@astro.as.utexas.edu; WWW: http://ncnc.as.utexas.edu/exes

2. SCIENCE GOALS

Our major goals for EXES involve high-resolution studies of interstellar molecules such as H_2, H_2O, and CH_4.[1] These molecules should be important diagnostics of the temperature, density, and dynamics of gas in molecular clouds, protostellar disks, and outflows.

Absorption line studies benefit from high resolution in several ways. By matching the resolution to the line width, we gain sensitivity. If we can resolve a line, we eliminate the need for a curve-of-growth analysis and its inherent uncertainties[3] and we gain access to kinematic information in the line shape. High resolution also makes it easier to separate terrestrial absorption from the astronomical features of interest. In Figure 1, we show a simulation of H_2O absorption observed with R = 10^5 and the wavelength coverage from a single EXES setting. We used the level populations from early ISO results[4] to simulate gas with $N_{H_2O} = 10^{18}$ cm^{-2} and temperatures of 25 K, 300 K, and 1000 K. Figure 1 indicates we should be able to separate atmospheric and terrestrial H_2O features, distinguish between populations with different temperatures, and resolve narrow line profiles.

High spectral resolution will also be critical to observations of H_2 emission near young stars. The Infrared Space Observatory (ISO) detected such H_2 emission in the two lowest pure rotational lines, the S(1) line at 17.035 μm and the S(0) line at 28.218 μm.[5] The lines were unresolved at R$\sim$2000, complicating the interpretation of whether the emission arose in a disk, an outflow, or a surrounding envelope. Each of these dynamically distinct cases should have a distinct line signature. Therefore, by spectrally resolving the emission, we should be able to identify the location of the H_2 emission. EXES on SOFIA will have superior sensitivity to ISO when looking at point sources with narrow lines.[1] From SOFIA, all the pure rotational H_2 lines from S(0) to S(9), with the exception of the S(3) line located within the ozone band at 9.66 μm, will be observable with EXES.

Although our interests in star forming and protostellar regions require only EXES's high resolution capability, the instrument design does not compromise the low and moderate resolution long-slit modes. With resolving powers of $\sim$4000, 2×10^4, and 10^5, high sensitivity, and the spectral access provided by SOFIA, EXES will prove a valuable tool for studies of planetary atmospheres, recombination lines, fine-structure lines, extragalactic PDRs, circumstellar envelopes, novae, and supernovae.

3. DESIGN

3.1. Optical Layout

3.1.1. Description

The basic EXES optical design has not changed from our earlier description[1]: focal reducing fore-optics, an echelon chamber, and a grating chamber with the cross-dispersion/long-slit grating (Figure 2). We follow the basic outline of our previous description of the optical design emphasizing new or modified elements. The fore-optics image the telescope secondary onto a cold pupil and reimage the telescope focal plane with 2:1 demagnification through a filter wheel onto a decker wheel and slit wheel. The echelon chamber contains the high dispersion echelon grating and its collimator/camera mirror. The grating chamber contains a diamond-machined echelle grating with groove quality such that both sides of the groove may be used, the collimator/camera mirror, focal reduction lenses, and the detector array.

EXES can be used in four different modes. In high resolution cross-dispersed mode (R $\approx$ 100,000), both grating chambers are used, with the echelle grating serving as the cross-disperser for the echelon. In medium resolution long-slit mode (R $\approx$ 20,000), the echelon chamber is not used and the echelle serves as the primary disperser. In low resolution long-slit mode (R $\approx$ 4000), the echelle grating is rotated past face-on so that the back sides of the grooves are used. In acquisition camera mode, the echelle grating is turned face-on to act as a low efficiency ($\eta \sim$10%) mirror. We describe the echelon in Section 3.1.3 and the echelle grating in Section 3.1.4.

The overall performance of the optical design is good. We are diffraction limited down to 8 μm with most of the aberration due to the focal reducing mirror in the foreoptics. The optics are sized such that we can upgrade our detector to a 512^2 pixel array without suffering in performance.

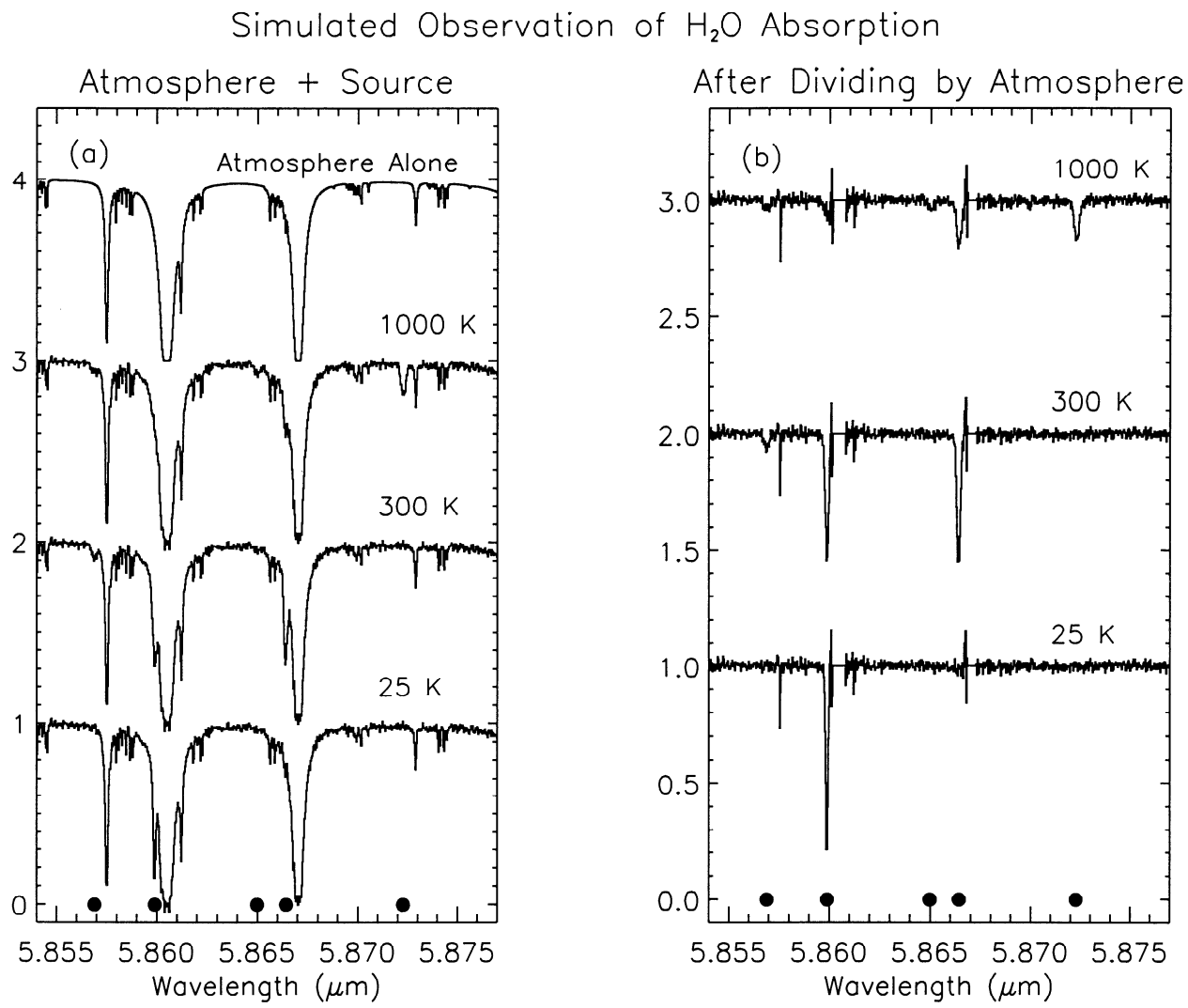

Figure 1. A simulated observation of H_2O absorption against a continuum source.[1] The wavelength range represents a single EXES setting. The continuum has signal-to-noise of 100:1. In all cases, the spectra are normalized to unity and an arbitrary constant is added for display. (a)The atmospheric transmission appropriate for 7 μm of precipitable water and 45° zenith angle is shown at the top. Subsequent curves represent absorption by a column with $N(H_2O)=10^{18}$ cm^{-2} and temperatures of T=1000, 300, and 25 K, respectively. We take a Doppler shift of -30 km s^{-1} to avoid telluric lines. The spectral resolution is $R=10^5$. (b)The same spectra after dividing by the atmosphere. In the simulation, our atmospheric reference source is assumed to have an infinite signal-to-noise.

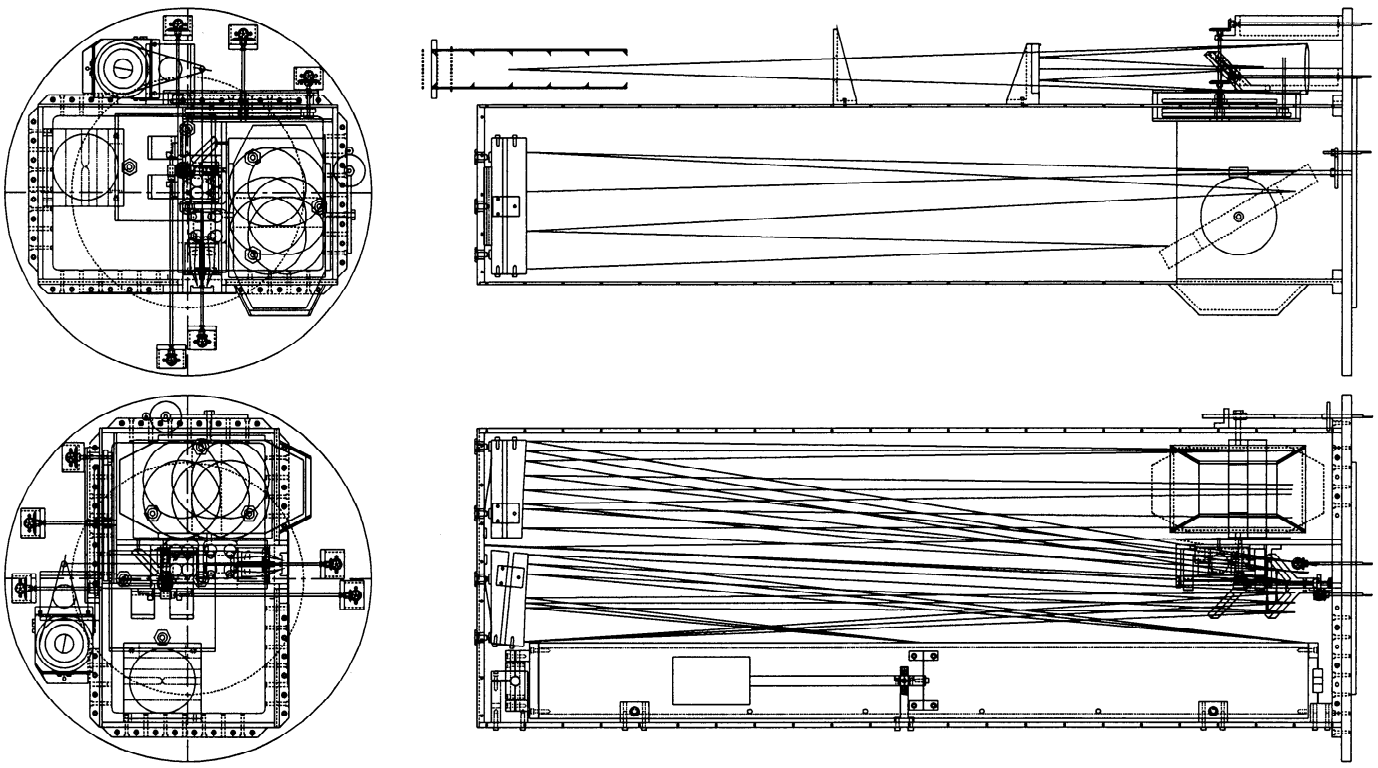

Figure 2. Four views of the optics. The top right view shows the foreoptics and the cross-dispersion chamber. The bottom right view shows the cross-dispersion chamber above the echelon chamber. On the left are end on views appropriate for the orientations on the right.

3.1.2. Fore-optics

Our entrance window is a field lens that images the telescope pupil on a LHe cold stop. An off-axis ellipsoidal mirror reimages the focal plane at f/10 before a pair of fold mirrors bring the light through the filter wheel and the decker wheel onto the slit wheel. We will use diamond-turned, gold-coated optics for all mirrors with power. The filter wheel houses 12 1-inch filters to isolate individual echelle grating orders. The combination of decker and slit wheels will give continuously adjustable slit lengths so that we can match the length to the order spacing provided in cross-dispersion. The decker wheel will also let us choose the out-of-plane, or γ, angle for the echelon. High blaze angle gratings have the (generally annoying) property that the diffraction angle for a given wavelength shifts substantially with out-of-plane incidence angle. With the echelon, this is a large enough effect that we can shift the blaze wavelength by $\sim$1/2 order by changing the position of the entrance aperture in the cross-dispersion direction (along the slit). In most cases, this shift will allow us to center the wavelength of interest on the echelon blaze, avoiding the loss in efficiency caused by splitting of the light between orders.

We are currently designing an entrance window/lens turret to hold three lenses optimized for different wavelength regions. The lens turret design is a response to the compromises imposed if trying to use a single lens material for operation at 5-25 μm. We will have one ZnSe lens with an antireflection coating appropriate for the 5-14 μm region. The other two lenses will be either CsI or KRS5 for operation beyond 16 μm. The turret rotates the unused lenses into a desiccated environment for protection. Design of the turret is complicated by the size, 8 inches diameter, and the fact that the rotating turret is part of the cryostat's vacuum seal. Since EXES will operate on both SOFIA and ground-based telescopes, the turret bearing and vacuum seal must function with external pressures of 0.1 atm to 1 atm. We envision a double O-ring and rotation on a thrust bearing, but have not finalized this design.

3.1.3. Echelon chamber

The echelon chamber consists primarily of the echelon grating, its collimator/camera off-axis paraboloid, and flat fold mirrors at the input and output of the chamber. The echelon is a 1 m long, 10 cm wide, R10 diffraction grating, with 7.62 mm groove spacing. It is used in very high order, from ≈3030 at 5 μm to ≈540 at 28 μm, to give large continuous wavelength coverage at R= 10^5.[2]

The echelon was diamond-machined by Hyperfine, Inc.[6] The 4 inch by 4 inch by 40 inch blank was cut from Aluminum 6061-T651 tooling plate. We specified that the blank come from the middle of the plate and that the grooves be cut from a face within the plate. A 3.5 inch hole was bored along the length of the blank to remove excess weight. After rough machining, we performed a stress-relief anneal following the standard prescription[7] to remove any residual stress in the blank. A slightly smaller grating blank (3.4 inches by 3.4 inches by 36 inches) was prepared following the same recipe; this grating, machined with the same groove parameters, is used in TEXES. After a number of test rulings, Hyperfine successfully machined the TEXES grating to our required tolerances. After each ruling, we examined the grating at room temperature using an optical interferometer setup that imaged individual grooves as well as a infrared spectrometer setup that could test subsections or the entire grating using either a CO_2 laser or a 3.4 μm HeNe laser. From these tests, in conjunction with 10.6 μm interferograms done by Hyperfine, Inc, we feel confident the gratings are diffraction limited to at least 7 μm. The TEXES grating has been tested at LHe temperatures in the TEXES dewar in the lab and at the telescope. The lab tests, using the infrared lasers as narrow line sources, showed the grating achieved R=10^5 while cold. The telescope results will be discussed in Section 6.

3.1.4. Grating chamber

The grating chamber houses an echelle grating, a collimator/camera mirror, a focal reduction lens, and the detector array. Since our last paper, we have decided to pursue a novel approach for the echelle grating. We plan on ordering a diamond-machined, R2.6 echelle grating with sufficient groove quality to operate to R1.1 with each groove acting as a retroreflector or at R1/3 as a low dispersion grating. By using the grooves as corner reflectors, the efficiency should be essentially independent on angle. Although we expect there to be polarization effects, we have modeled the retroreflector grating and find its efficiency to be quite good. In fact, the current TEXES echelle cross-disperser is a conventional R4 grating that we choose to use mostly at R2 and below with no loss of efficiency. Diamond-machining should be able to produce a grating with high quality surfaces on both sides of the grooves. We are currently determining the optimal groove spacing for our needs: certain "popular" wavelengths would ideally be available at two grating settings so that the resolution can be matched to the science.

A focal reduction lens is required to match the slit image to the detector. Our detector has 30 μm pixels. At 10 μm, the diffraction spot, $f\lambda$, is 100 μm across without any focal reduction. Therefore, we will speed up the beam from f/10 to f/6. The lens, made of either CsI or KRS5, will be on a translation stage to correct for chromatic aberration. With the lens immediately before the detector, other aberrations are minimized. By moving the lens to the extreme end of its motion, we will will be able to image the cold pupil of the instrument.

3.2. Mechanical and Cryogenic Design

The dewar design is shown in Figure 3 Our description here emphasizes elements of the design not presented previously.[1] Its outer wall is an 24 inch diameter, almost 80 inch long cylinder (including mounting ring). We estimate the cryostat mass to be 500 lbs.

One new element of our design is that the cryogen reservoirs are now at the forward (away from the telescope) end of the cryostat. This will enable us to fill the cryogen reservoirs without removing the instrument from its mounting flange. The reservoirs have rounded endcaps, except at the LHe work surface, to increase the strength-to-weight ratio. The fill tubes are offset on the reservoirs so that the cryostat can be tilted beyond horizontal without spilling its cryogens. The fill tubes will have coaxial neck tubes to provide redundant paths for escaping cold gas. Each reservoir has a maximum capacity of ~10 liters. We expect the LHe hold time to be 2-3 days while the LN_2 hold time should be 1-2 days.

Given the size of our cryostat, room temperature radiation from the vacuum jacket will produce the largest heat load on the LN_2. To reduce this heat load, our outermost radiation shield will be a floating shield; it will be thermally isolated from the cryogen reservoirs with G10 fiberglass. In theory, a floating shield cuts the heat load in half. We will also thermally link the cyrogen necks to the floating shield to remove some heat with the cryogen

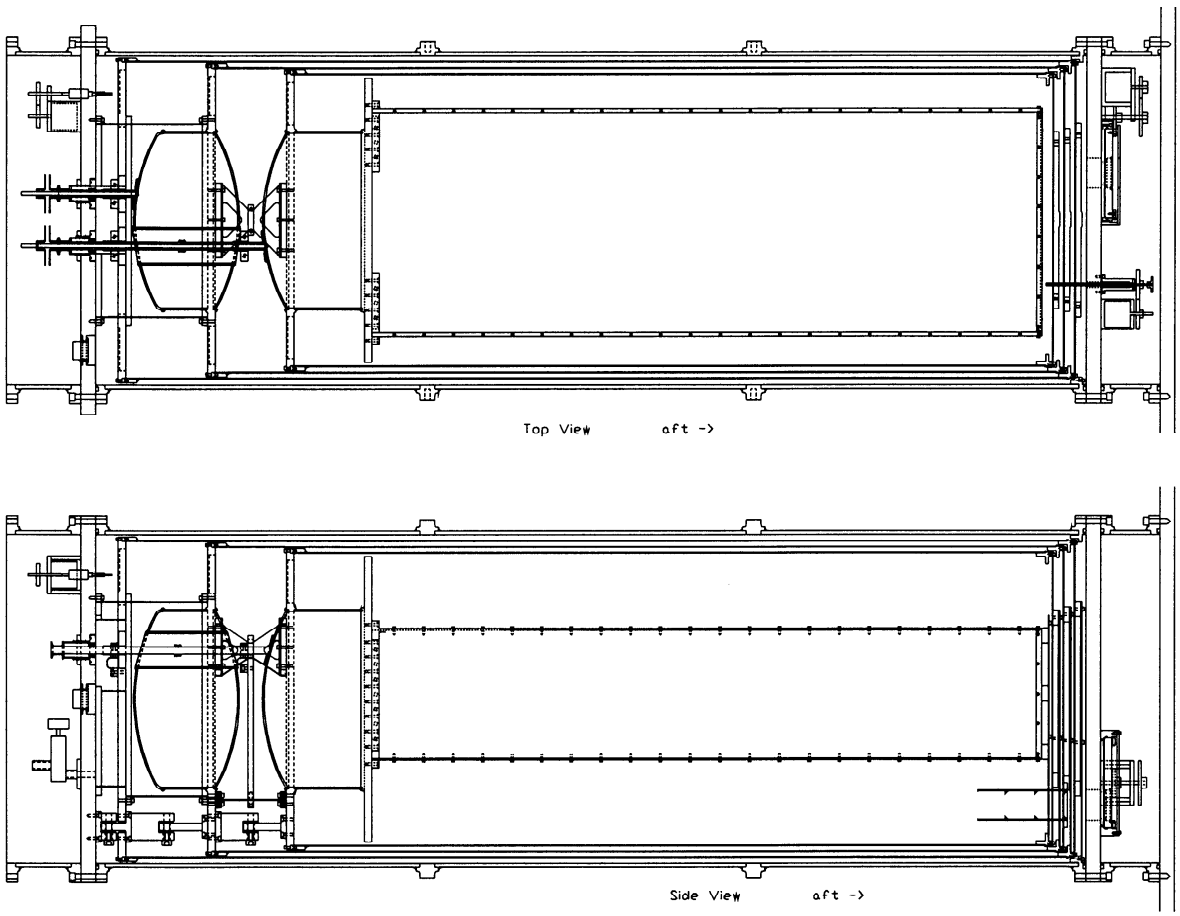

Figure 3. Two views of the EXES cryostat with no optics shown.

boiloff. Similarly, the G10 connections between the LHe and LN_2 reservoirs, a major heat load on the LHe layer, will be thermally tied to the LHe neck to utilize those cold vapors.

While the fiberglass support between the room temperature vacuum jacket and the floating shield, and between the floating shield and the LN_2 reservoir can afford to be quite substantial since radiation will be the dominant heat load, the G10 supports between the LN_2 and LHe reservoirs need to be optimized. We have chosen to use three G10 "Xs" (see Figure 4) Using numerical modeling of the heat flow and actual mechanical testing of a half-scale prototype, we expect EXES's Xs to significantly improve the LHe hold time compared to rectangular G10 tabs.

The basic design is a fiberglass square with the fibers oriented along the diagonal. We then notched out the left and right sides of the x and cut holes in the top and bottom (see Figure 4) To prevent buckling at the midpoint of the Xs, we will link all three Xs with an aluminum plate. This plate will also thermally tie the G10 to the helium neck. We epoxied multiple layers of thin fiberglass to form the support's base. In our prototype, we placed these epoxied layers on only one side of the X. Our stress tests repeatedly showed that the epoxy on the support base failed long before the fiberglass. By sandwiching the Xs between two epoxied blocks and screwing both sides down to the base plate we expect the pieces to be much stronger. Our stress measurements showed the Xs were only a factor of two weaker than a square fiberglass tab while numerical calculations suggest the heatflow is decreased by a factor of almost 6, giving a net improvement in the strength-to-heatflow ratio of a factor of nearly 3.

While the G10 supports will be sufficient for normal operating loads, we have backup mechanical supports for the ultimate load cases required by SOFIA and for shipping. These stainless steel supports consist of a fork with a pin. There are three supports at each layer: vacuum jacket to floating shield, floating shield to LN_2 reservoir, and LN_2 reservoir to LHe reservoir. The pin is undersized so that there is a 1 mm gap and no thermal contact.

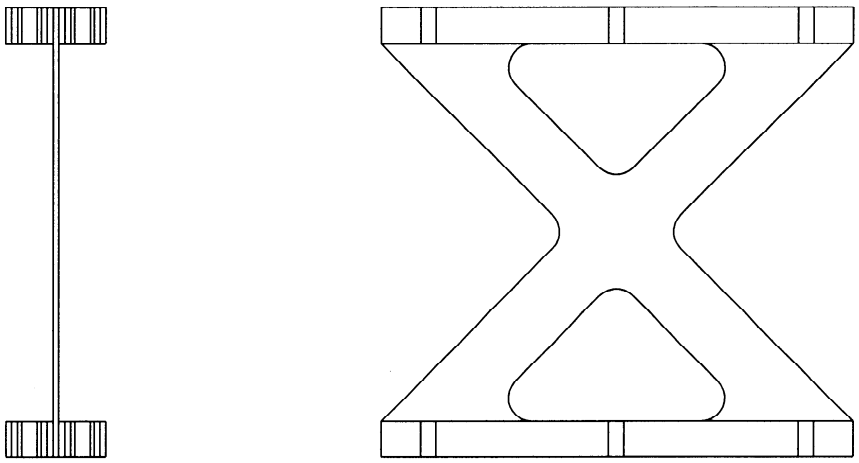

Figure 4. The design of the G10 "Xs". The fibers run along the axes of the Xs. The Xs have a 4 inch by 4 inch envelope.

Ideally, the pins will engage just as the fiberglass nears its elastic limit. When shipping the cryostat, the undersized pins are replaced with slip-fit pins so that the G10 supports are not used at all. As an additional precaution, we have minimized the gap between radiation shields to 1/16 inch so that substantial loads will be distributed over the contact area between shields as well as the G10 supports and the fork-and-pin supports.

4. DETECTOR AND ELECTRONICS

Our choice of detector array is driven by the core science goals involving high spectral resolution at 5.5 μm$\leq \lambda \leq$ 7 μm. The combination of high spectral resolution, short wavelengths, and detector response as a function of wavelength results in a low rate of background electrons. The number of electrons generated by background sky photons [e^- s^{-1} pixel^{-1}] can be taken as

$$N_{e^-} = \frac{\varepsilon \lambda^2 B_\lambda(T) A \Omega}{hcR} \eta_{opt} \eta_{det} \quad (1)$$

where ε is the emissivity (telescope + sky), λ is the wavelength of interest, $B_\lambda(T)$ is the Planck function evaluated at the telescope temperature, A is the telescope area, Ω is the solid angle seen by a pixel, h is Planck's constant, c is the speed of light, R is the resolving power of the spectrograph, η_{opt} is the optical efficiency of the instrument, and η_{det} is the quantum efficiency of the detector. Taking $\varepsilon = 0.15$, $\lambda = 6$ μm, $T = 245$ K, $A = 49,000$ cm^2, $\Omega = 0.16$ square arcseconds, $R = 10^5$, $\eta_{opt} = 0.2$, and $\eta_{det} = 0.4$, we find a background count rate of 330 e^- s^{-1} pix^{-1}. To ensure our instrument is background noise limited, we must have a detector with very low read noise.

We chose the Raytheon 256^2 Si:As IBC "SIRTF" array with the CRC-744 readout integrated circuit. We received our science grade array in December 1999. According to the tests results prepared by Raytheon, the mean read noise measured 15.6 e$^-$ with 4 Fowler pairs, which meets our requirements for the high resolution mode. The quantum efficiency measured at 7.74 μm is almost 50%. We expect the detector will have ~10% quantum efficiency at 28.3 μm, the wavelength of the H_2 S(0) line. The pixel-to-pixel variations in quantum efficiency are $\pm$3% (1σ). The well size is $\approx$ 190,000 e$^-$ at 1.0 V reverse bias. This, combined with a maximum frame rate of 20 Hz, poses some problems when operating at low resolution or camera mode. We discuss our attempts to solve these problems as well as our experiences with the array at the telescope in Section 6.

To run our detector, we purchased a version of the IR Observer^{TM} electronics system from Wallace Instruments. The system includes an analog box with clock driver boards, DC bias boards, and preamp boards; a digital box with timing pattern control boards, coadder control boards, 14-bit analog-to-digital converters, and coadder memory chips; a rack-mounted control computer running Linux; a rack-mounted power supply; and all the cables required to

interface the system with the cryostat. The system came equipped with software suitable for lab testing; we describe some of the modifications required for use at the telescope in Section 6.

Two levels of EPROM programs contain the basic clocking information. The "Master" EPROM, a single 8 bit by 256 k chip, contains a series of starting addresses for separate slave routines. The five 8 bit by 256 k "Slave" EPROMs operate in parallel and control the clocking levels, the coadder synchronization, and can control a chopping secondary. The hardware can contain up to 32 slave patterns and 32 master patterns. The patterns currently programmed into the EPROMs include a correlated double sampling (CDS) mode, a simple read and reset mode, and a partial array readout in CDS. If more than 32 patterns are needed, additional EPROM chips must be programmed and inserted into the control board.

As much as possible, we will strive for commonality between our ground-based instrument, TEXES, and EXES. Although the 256^2 detector is the maximum size possible in TEXES, EXES is designed to fit a 512^2 array. The Wallace electronics should be able to run such an array with minimal changes.

5. SOFTWARE

The software for EXES will have two relatively isolated sides: a data taking and instrument control side running in Tcl/tk and C on the Linux computer provided with the Wallace Instruments electronics package; and a data quicklook and reduction pipeline running in IDL on Sun workstations. Both sides will function as either graphical user interfaces (GUI) or command line inputs to facilitate the use of macros.

The IROBS software interface furnished by Wallace Instruments uses a GUI to control the array and to display the results of a readout. The GUI is written in Tcl/tk with specialized Tcl commands added via C programs. It arrived capable of writing FITS files with minimal headers. In practice, we found the Tcl/tk fairly easy to understand and modify. We have incorporated command line routines for telescope control, overall instrument control, setting and displaying header information, and storing the data in our desired format: binary data files with three dimensions and separate text headers. Much work remains to make the GUI a complete instrument controller, although we plan to build our efforts on top of the command line routines already instituted.

The complexity of cross-dispersed spectral data indicated to us early on that we would need a fairly fast, extendable, and versatile quicklook software package. We chose IDL as the platform because of its ability to operate on and display data arrays. We wrote command line driven routines that met the basic requirements for operation at the telescope and then began building those routines into a GUI using IDL Widgets. The quicklook contains a simple model of the instrument so that a synthetic spectrum can be produced using a model of the terrestrial atmosphere. With refinement over time, we expect the instrument model to be accurate to the few pixel level or better. Many of the quicklook routines will be incorporated into a pipeline data reduction once we have a good understanding of how to reduce the data.

The connection between the two sides of the software is currently quite unsophisticated. The data taking computer writes the data to its disk in a directory specified by the user. The Sun workstation running the quicklook mounts this disk and so is able to read the data files as they come in. We presently use a intermediary file that the quicklook software reads repeatedly to determine when there is new data. Eventually, we will establish a proper handshake between the data taking software and the quicklook using a socket connection.

Since EXES is not a facility class instrument, we do not require our GUIs to be completely user-friendly. We fully expect the software to be unusable by individuals unfamiliar with our instrument. A requirement on our pipeline reduction, though, is the production of FITS files with sufficient integrity that our collaborators have easy access to reduced data in a format that should be suitable for their needs.

6. TELESCOPE EXPERIENCE

We have just returned from a successful telescope run on McDonald Observatory's 2.7 m Harlan J. Smith Telescope with our ground-based instrument, TEXES. Our telescope run was for a mixture of engineering and science projects. We used TEXES in all four of its modes and proved that the different modes could be called upon with little operational overhead. We show some samples of the raw data collected in Figures 5 and 6. Much work remains to be done to properly reduce the data. A rough estimate of the overall instrument efficiency, including detector, is ~10%, in line with prior our expectations. Given that we do not have a determination of the EXES sensitivity, we refer the reader to our previous paper[1] for sensitivity estimates.

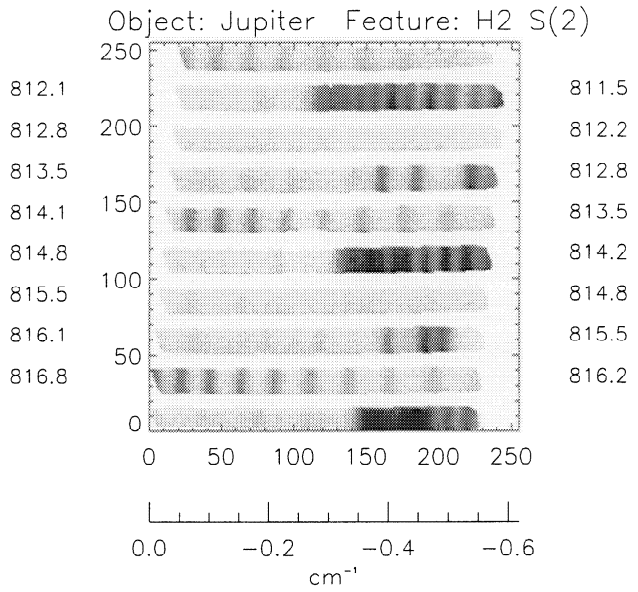

Figure 5. A high-resolution, cross-dispersed spectrum of Jupiter at 814 cm^{-1}. Although the feature of interest was the H_2 S(2) line, nearly all the emission lines present are bands of C_2H_6. Echelon dispersion runs horizontally with orders stacking vertically. In general, the orders and slit images do not line up with the rows and columns on the array; the quicklook software rotates the image based on the model of instrument and knowledge of the echelle angle. Each order is labeled with approximate first and last wavenumbers with a dispersion scale displayed below. This spectrum has been divided by a flatfield to remove the blaze function and terrestrial absorption. The greyscale intensity units, although arbitrary at this point, run from white (0) to black (1).

The performance of the echelon grating is quite good in terms of efficiency and resolution. We estimate the efficiency of the echelon at the peak of the blaze function is ~80%. The resolution can best be seen in a lunar spectrum with absorption by terrestrial ozone (Figure 7). In the figure, we show the data from one order along with the convolution of a model atmosphere with a dispersion profile (Lorentzian) with FWHM of .01 cm^{-1}. Thus, our resolving power is 100,000.

The detector performed very well. At low background levels, in high-resolution mode, the integration time must be set to ensure background limited performance, around 1000 e^- in a correlated double sampling scheme. Future implementation of a multiple sampling scheme will be necessary for SOFIA. To avoid saturation in camera and low resolution mode, we used a 64 row by 256 column (spatial by spectral) readout scheme that allows shorter integration times. The medium resolution long-slit mode is in danger of saturating on strong atmospheric lines at $\lambda > 12$ μm. Since the slit does not cover the full array, we will want to match a partial array readout to the slit length. During the run, we adapted the software to warn us if the background counts were either too high or too low.

Some array behaviors still puzzle us. During a partial array readout, all rows are reset, but only the central 64 rows are read and reset. When we returned to a full frame, the central 64 rows had a systematically higher (less negative) reset level. This memory persisted with a halflife on the order of 10 minutes. If we turned the power to the array off for one minute, the array returned to normal operation. Although the array behaves well at low light levels, the noise increases beyond the photon shot noise at high light levels. There seems to be a photon flux threshold above which more and more pixels have more noise than expected. We believe this will affect our sensitivity in low resolution mode.

We can make considerable improvements in observing efficiency by modifying the electronics and software. One of our greatest inefficiencies is the amount of time lost when nodding the telescope. On some observations, our duty cycle was 50%. By upgrading two electronics boards to a faster bus speed, by writing software to change the master

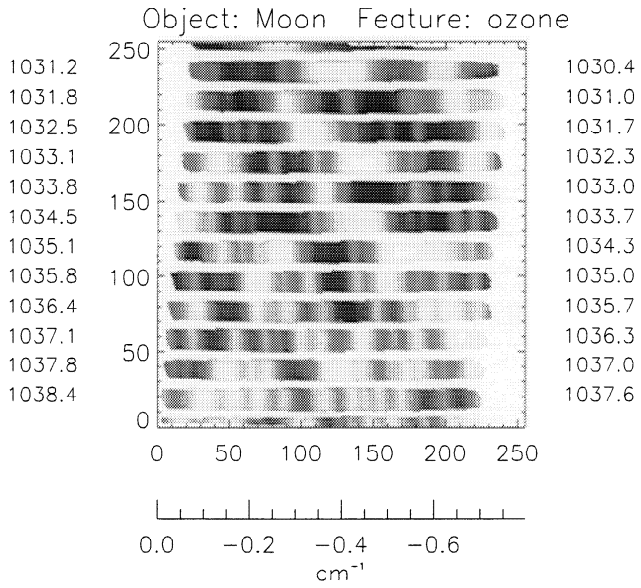

Figure 6. A high-resolution, cross-dispersed spectrum of the moon with terrestrial ozone absorption. The spectrum has been divided by a flatfield to remove the echelon blaze function. The greyscale intensity units, although arbitrary at this point, run from white (totally absorbed) to black (lunar continuum).

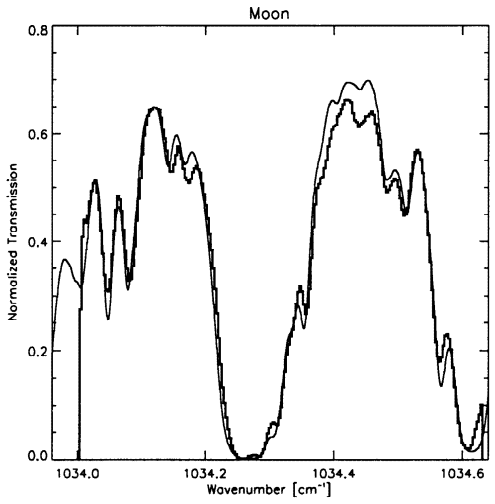

Figure 7. The lunar spectrum with absorption by terrestrial ozone. One echelon order is shown. The thick line is the data while the thin line is the convolution of a model Earth atmosphere with a dispersion profile (Lorentzian) with FWHM of 0.01 cm^{-1}. The data were corrected for scattered light by bringing the strong absorption to zero.

clock pattern on the fly, and by establishing a fast handshake between the data taking and quicklook software, we can bring our lost time down to the time it takes the telescope to settle.

Efficiency can also be gained by faster instrument control and preventing operator errors. When EXES is flying on SOFIA, the user will be able to enter the desired instrument mode (e.g. hires) and the desired wavelength and then expect the instrument to configure itself properly; the software will have enough knowledge of the instrument to rotate the proper optics into position, set the proper array readout parameters, and store this information into the header. The user will have the ability to override the suggestions from the software, but the software should be reasonable suggestions most of the time.

7. CONCLUSION

EXES will provide a unique platform for studying mid-infrared molecular lines at many wavelengths unavailable from the ground. For very extended objects, EXES will have line-flux sensitivity comparable to ISO's Short Wavelength Spectrometer (SWS) Fabry-Perot system, but with 10 times the spectral and spatial resolution. On point sources, EXES should be as sensitive to the continuum as the ISO SWS in grating modes, but with 50-100 times the spectral resolution. The mid-IR spectrometer on SIRTF will undoubtedly have much better sensitivity than we can achieve, but will have a resolution ($R \leq 600$) much lower than ours. At those wavelengths where our ground-based instrument can observe on Gemini, the gain in sensitivity that results from the lower telescope temperature of SOFIA is too small (factor of $\sim$2 for extended objects; factor of $\sim$0.2 for point sources) to justify observations at wavelengths with acceptable atmospheric transmission from Mauna Kea. Rather, we conclude that the sensitivity achievable on SOFIA is comparable to that achievable on the largest ground-based telescopes, allowing us to observe the same sources as would be observed by Gemini at wavelengths inaccessible from Mauna Kea. EXES will be uniquely capable of the high-resolution, high-sensitivity mid-IR observations required to study molecules in many astronomical environments.

ACKNOWLEDGMENTS

This work is sponsored by grant USRA 8500-98-008.

REFERENCES

1. M. J. Richter, J. H. Lacy, D. T. Jaffe, M. K. Hemenway, and W. Yu, "EXES: an echelon cross echelle spectrograph for SOFIA," *Proc. SPIE* **3354**, pp. 962–972, Aug. 1998.
2. J. H. Lacy, M. J. Richter, W. Yu, and B. S. Basso, "Texas echelon cross echelle spectrograph," *Proc. SPIE* **3354**, pp. 436–447, Aug. 1998.
3. J. S. Carr, I. Evans, N. J., J. H. Lacy, and S. Zhou, "Observation of infrared and radio lines of molecules toward GL 2591 and comparison to physical and chemical models," *ApJ* **450**, pp. 667+, Sept. 1995.
4. F. P. Helmich, E. F. van Dishoeck, J. H. Black, T. de Graauw, D. A. Beintema, A. M. Heras, F. Lahuis, P. W. Morris, and E. A. Valentijn, "Detection of hot, abundant water toward AFGL 2591," *A&A* **315**, pp. L173–L176, 1996.
5. W. F. Thi, E. F. van Dishoeck, G. A. Blake, G. J. van Zadelhoff, and M. R. Hogerheijde, "Detection of H_2 pure rotational line emission from the GG Tauri binary system," *ApJ* **521**, pp. L63–L66, Aug. 1999.
6. K. G. Bach, B. W. Bach, and B. W. J. Bach, "Large ruled monolithic echelle gratings," *Proc. SPIE* **4014**, p. 000, Aug. 2000.
7. R. H. Gassner, C. H. Avery, H. H. Block, J. R. Douslin, V. E. Dress, R. E. Huffaker, R. D. Kesler, T. I. McClintock, G. R. Moudry, C. A. Rosellen, R. Schmidt, E. Stair, M. M. Tilley, and J. C. White, "Heat treating of aluminum alloys," in *Metals Handbook*, T. Lyman, ed., pp. 271–283, American Society of Metals, Metals Park, 1964.